

Secreted autotaxin through LPA suppresses chemotaxis and tumor infiltration of CD8⁺ T cells

Elisa Matas-Rico¹, Irene van der Haar Avila², Maaïke van Zon³, Andrew J. Morris⁴, Jan Koster⁵, Fernando Salgado-Polo^{1,6}, Sander de Kivit^{2,6,11}, Iris de Rink⁷, Telma Lança^{3,12}, Juan Manuel Alba⁸, Zoë Johnson⁹, Stuart Farrow¹⁰, John Haanen³, Ton N. Schumacher^{3,6}, Anastassis Perrakis^{1,6}, Jannie Borst^{2,6,11}, Inge Verbrugge², Joost van den Berg³, Wouter H. Moolenaar^{1,*}

¹ Division of Biochemistry, ² Division of Tumor Biology and Immunology, ³ Division of Molecular Oncology and Immunology, Netherlands Cancer Institute, Amsterdam, The Netherlands

⁴ Division of Cardiovascular Medicine, Gill Heart Institute and Lexington Veterans Affairs Medical Center, University of Kentucky, Lexington, KY, USA

⁵ Amsterdam UMC, Department of Oncogenomics, Amsterdam, The Netherlands.

⁶ OncoCode Institute, The Netherlands

⁷ Genomics Core Facility, Netherlands Cancer Institute, Amsterdam, The Netherlands

⁸ Evolutionary and Population Biology-IBED, University of Amsterdam, Amsterdam, The Netherlands

⁹ iOnctura SA, Campus Biotech Innovation Park, Geneva, Switzerland

¹⁰ CRUK Therapeutic Discovery Laboratories, London, UK

¹¹ Present address: Department of Immunohematology and Blood Transfusion, Leiden University Medical School, Leiden, The Netherlands

¹² Present address: Technical University of Denmark, Department of Health Technology, Lyngby, Denmark

* e-mail: w.moolenaar@nki.nl

Summary

To improve immunotherapy efficacy, a better understanding of the factors that regulate T-cell migration into tumors is essential. Here we uncover a role for autotaxin (ATX) in this process. ATX (encoded by *ENPP2*) produces lysophosphatidic acid (LPA) that activates G protein-coupled receptors (LPAR1-6) to regulate multiple (patho)physiological processes, including tumor progression via LPAR1 and lymphocyte homing via LPAR2. Unexpectedly, we find that melanoma cell-secreted ATX is a major chemorepellent for tumor-infiltrating lymphocytes *ex vivo* through $G\alpha_{12/13}$ -coupled LPAR6, with ATX functioning as an LPA-producing chaperone. Using an anti-cancer vaccination model, we provide proof-of-concept that secreted ATX opposes tumor infiltration of CD8⁺ T cells. Additionally, *ENPP2* expression in melanoma tumors correlates with reduced CD8⁺ T-cell infiltration as inferred from single-cell transcriptomics. Hence, by counteracting T-cell infiltration while activating tumor cells via different LPA receptors, the ATX/LPA complex exerts dual actions in the tumor immune microenvironment, which may provide new therapeutic approaches.

Introduction

One determinant of positive immunotherapy outcome is the efficient infiltration of T cells into the tumor (Chen and Mellman, 2013; Fridman et al., 2017; Giraldo et al., 2019; Sharma and Allison, 2015). However, our understanding of the factors that dictate the trafficking of tumor-infiltrating lymphocytes (TILs), either positively or negatively, is incomplete and requires identification of new tractable targets (Anandappa et al., 2020; Sackstein et al., 2017; van der Woude et al., 2017). Chemokines through their G protein-coupled receptors (GPCRs) are major drivers of T-cell chemotaxis and trafficking and keep attracting interest as potential therapeutic targets in immuno-oncology (Chow and Luster, 2014; Do et al., 2020; Vilgelm and Richmond, 2019). Tumors evolve various strategies to evade T-cell infiltration via activation of oncogenic signaling pathways, for instance by suppressing chemokine production and signaling and/or by secreting anti-migratory molecules such as Wnt ligands and TGF β (Batlle and Massague, 2019; Hinshaw and Shevde, 2019; Keridani et al., 2019; Spranger et al., 2015). Yet, much remains to be learned about soluble factors and GPCR ligands that counteract T-cell chemotaxis and tumor infiltration. Here we explore a role for autotaxin (ATX) in this process.

ATX (encoded by *ENPP2*) was identified as a melanoma cell-secreted motility factor with angiogenic and metastasis-enhancing capacity (Nam et al., 2001; Stracke et al., 1992). ATX is a lysophospholipase D (lysoPLD) that produces the GPCR agonist lysophosphatidic acid (LPA) from extracellular lysophosphatidylcholine (LPC), an abundant plasma phospholipid (Perrakis and Moolenaar, 2014; Tokumura et al., 2002; Umezue-Goto et al., 2002). ATX/LPA plays a key role in a wide variety of

(patho)physiological processes, including vascular development (van Meeteren et al., 2006), lymphocyte homing (Kanda et al., 2008), pulmonary fibrosis (Tager et al., 2008) and tumor progression (Benesch et al., 2018; Mills and Moolenaar, 2003). LPA signals through six GPCRs, termed LPAR1-6 or LPA₁₋₆, showing both distinct and overlapping signaling activities (Yanagida et al., 2013; Yung et al., 2014). LPAR1-3 belong to the EDG family of GPCRs together with the sphingosine 1-phosphate (S1P) receptors, whereas the disparate LPAR4-6 members are related to the purinergic receptors (Hisano and Hla, 2019; Yanagida et al., 2013).

Numerous studies have documented a critical role for ATX and/or LPA in stimulating (tumor) cell migration, dispersal, invasion, tissue repair and metastasis, mediated primarily by LPAR1 (Auciello et al., 2019; David et al., 2010; Lin et al., 2019; Liu et al., 2009; Marshall et al., 2012). LPAR1 also mediates the activation of fibroblasts, a prototypic ATX-secreting cell type whose aberrant activation leads to life-threatening tissue fibrosis (Tager et al., 2008). In contrast to LPAR1-3, non-EDG receptors LPAR4-6 have been reported to suppress the migration of both normal and malignant cells (Jongsma et al., 2011; Lee et al., 2008; Takahashi et al., 2017). In the immune system, ATX is abundantly expressed in high-endothelial venules (HEVs) that control lymphocyte entry into lymphoid tissue (Kanda et al., 2008; Takeda et al., 2016). Through LPA production, HEV- and lymphoid stroma-secreted ATX promotes the random motility – but not their chemotaxis - of naïve T cells to enhance their transmigration from blood into lymphoid tissue and sustain their motility within lymph nodes via LPAR2 (Bai et al., 2013; Kanda et al., 2008; Knowlden et al., 2014; Takeda et al., 2016). The pro-metastatic ATX-LPAR axis thus regulates the migratory activities of both tumor and T cells; however, its actions in the tumor immune microenvironment remain unclear

Here we report that secreted ATX antagonizes the chemotactic migration of *ex vivo* expanded TILs and peripheral CD8⁺ T cells, and uncover ATX as an LPA-producing chaperone. We show that secreted ATX opposes tumor infiltration of CD8⁺ T cells *in vivo* and, furthermore, provide correlative clinical evidence for intratumoral ATX repelling CD8⁺ T cells in melanoma through single-cell analysis. By uncovering a negative immune regulatory role for the pro-metastatic ATX-LPAR axis, our findings shed new light on its multifaceted actions in the tumor microenvironment, suggesting new therapeutic approaches.

Results

ENPP2 expression in cancer cells versus solid tumors. Across >1000 cancer cell lines from 38 distinct cancer types (Ghandi et al., 2019), melanoma cell lines (n=61) stand out for their high median expression of ATX-encoding *ENPP2* (**Suppl. Fig. S1A**). This high *ENPP2* expression is unrelated to gene amplification or activation of oncogenic

pathways (<https://www.cbiportal.org>) but rather reflects high ATX expression observed in normal melanocytes (Filipp et al., 2019) and results not shown). Remarkably, however, *ENPP2* expression in cancer cells correlates rather poorly with that in the corresponding tumors (**Suppl. Fig. S1A,B**). In fact, *ENPP2* is abundantly expressed virtually in all solid tumors (**Suppl. Fig. S1B**). This implies that a substantial part of the tumor *ENPP2* transcripts originates from ATX-expressing stromal cells - notably cancer-associated fibroblasts - depending on the cancer type, a notion supported by single-cell analysis of melanoma tumors (see below) and exemplified by analysis of stroma-rich pancreas tumors (Auciello et al., 2019).

Through LPA, melanoma cell-secreted ATX is chemorepulsive for TILs and peripheral CD8⁺ T cells. We set out to examine how melanoma cell-secreted ATX affects the migration of *ex vivo* expanded melanoma TILs and peripheral CD8⁺ T cells. Melanoma TILs constitute a heterogeneous population of T cells in distinct functional states and other immune cells (Li et al., 2019). During their *ex vivo* expansion using IL-2 and anti-CD3, TILs become strongly enriched in CD8⁺ and CD4⁺ T cells and are then used for adoptive TIL therapy in patients. We first analyzed the effects of LPA and ATX/LPC on the transwell migration of TILs (isolated from two patients), using chemokine CXCL10 as positive control. Strikingly, LPA(18:1) strongly suppressed the basal migration rate of TILs (up to 5-fold in patient #1) when assayed over a period of 2 hrs, in a dose-dependent manner (**Fig. 1A,B**). LPA was capable of antagonizing TIL migration towards CXCL10, which signals through CXCR3 (**Fig. 1C**). LPA was also chemo-repulsive for peripheral blood CD8⁺ T cells isolated from healthy donors (**Fig. 1D**). It is noteworthy that peripheral CD8⁺ T cells were consistently more responsive to CXCL10 than melanoma TILs, suggesting that *ex vivo* expanded TILs have lost chemokine signaling efficacy. Loss of essential functions (“dysfunction”) in TILs during tumorigenesis is commonly observed (Thommen and Schumacher, 2018), but seemingly does not affect LPA responsiveness. As predicted, when TILs or CD8⁺ T cells were exposed to recombinant ATX (20 nM) together with its substrate LPC (1-5 μ M), their transwell migration was similarly suppressed (**Fig. 1E**).

We next examined melanoma supernatants for their T-cell migration-modulatory activity, concurrently with secreted ATX protein and lysoPLD activity. Culture media (containing 0.5% serum) conditioned by independent melanoma cell lines (MDA-MB-435 and A375) for 24 hrs showed marked suppression of the spontaneous migration and CXCL10-induced chemotaxis of TILs and peripheral CD8⁺ T cells (**Fig. 2A**). ATX was readily detected in these media (**Fig. 2B**), while secreted lysoPLD activity accumulated simultaneously (**Fig. 2C**). By contrast, conditioned media from ATX knockdown melanoma cells or ATX-deficient MDA-MB-231 breast carcinoma cells lacked chemo-repulsive activity (**Fig. 2D-F**). TILs migration could be rescued by incubating melanoma media with unrelated small-molecule ATX inhibitors, namely PF-8380 (Gierse et al., 2010)

and IOA-289 (formerly CRT750; (Shah et al., 2016)) (**Fig. 2G**). These results demonstrate that ATX through LPA production is the major, if not only, T-cell repellent secreted by melanoma cells.

LPA evokes a unique gene expression signature in TILs. Next, we asked whether LPA may induce additional responses in TILs besides inhibiting their migration. In non-immune cells, LPA and other GPCR agonists induce a gene expression program leading to altered long-term cell behavior, largely secondary to RhoA-mediated actin remodeling (Esnault et al., 2014; Stortelers et al., 2008; Yu et al., 2012). We examined the differentially expressed early genes in LPA-treated TILs (from both patients). Bulk RNA sequencing (RNA-seq) of TILs revealed differential expression (>2-fold) of more than 200 genes within 2 hrs of LPA treatment, showing marked differences between both patient samples with an overlap of about 30% (**Suppl. Fig. S2A** and results not shown). Common LPA-induced early genes included key transcription factors, T-cell regulatory surface molecules and cytokine receptors (**Suppl. Fig. 2A,B**). However, this early transcriptional response to LPA did not translate to altered TIL phenotypes (**Fig. 2C**), neither did LPA treatment affect tumor recognition by TILs, as inferred from the production of interferon-gamma (IFN- γ) upon co-incubating TILs with matching autologous melanoma cells (**Fig. 2D**). Nonetheless, further exploration of this early gene expression signature is warranted as it may reveal new ATX/LPA-regulated T-cell functions besides migration inhibition.

Depletion of LPA by melanoma cells reveals ATX as an LPA-producing chaperone.

LPA exists as distinct molecular species that differ in their acyl chain composition and binding affinity for individual LPA receptors (Yung et al., 2014). We measured LPA species in the respective media from melanoma cells conditioned at 0, 24 and 48 hrs by using LC-MS/MS (Kraemer et al., 2019). As shown in **Fig. 3A**, LPA(12:0), (16:0), (18:0), (18:1) and (20:4) were identified as the predominant species in media containing 0.5% serum (note: at this low concentration, serum has not effect on T-cell migration; cf. **Fig. 1D,E**). Contrary to our expectations, steady-state LPA levels in TIL-repulsive media declined to physiologically insignificant levels within 24 hrs - with LPA(18:0) being most resistant to depletion – despite the fact that ATX levels and lysoPLD activity increased concurrently (**Figs. 3B,C** and **2A,B**). This rapid depletion of extracellular LPA is attributable to LPA breakdown by ubiquitous cell-associated lipid phosphate phosphatases (LPP1-3) (Sciorra and Morris, 2002). It thus appears that LPA-producing ATX activity is outperformed by LPA-degrading activity. Yet, ATX is bioactive at steady-state LPA levels well below the approx. 100 nM needed for significant LPAR activation (Choi et al., 2010). That ATX is bioactive physiologically insignificant LPA levels can be explained by the fact that ATX binds LPA in its ‘tunnel’ or ‘channel’, located close to the active site (Keune et al., 2016; Moolenaar and Perrakis, 2011; Nishimasu et al., 2011; Salgado-Polo et al., 2018). As such, ATX functions as an LPA-producing chaperone that protects LPA from rapid degradation and delivers it to its cognate receptors ensure optimal signaling

TIL repulsion mediated by LPAR6. We examined the LPAR expression repertoire in TILs and CD8⁺ cells. *Ex vivo* expanded melanoma TILs (from three patients) express high levels of *LPAR6* in addition to considerably lower levels of *LPAR2* (**Fig. 4A**). An identical LPAR expression pattern was found in ovarian carcinoma-derived TILs (results not shown). *LPAR6* was also predominant in peripheral CD8⁺ T cells, alongside *LPAR2*, *LPAR4* and *LPAR5* (**Fig. 4B**). *LPAR4* and *LPAR5* may have been lost from TILs due to specific tumor micro-environmental conditions and/or during their *ex vivo* expansion. *LPAR6* (formerly *P2RY5*) couples to the $G\alpha_{12/13}$ -RhoA pathway that drives F-actin remodeling, cytoskeletal contraction, suppression of cell motility and other cellular responses (Inoue et al., 2019; Wu et al., 2019; Yanagida et al., 2009; Yung et al., 2014). Its function in T cells has remained unexplored to date, despite its abundant expression in immune cells (**Fig. 4C**). In contrast to *LPAR6*, *LPAR2* couples to G_i -mediated Rac GTPase activation and other G protein-effector routes, thereby promoting the random motility of T cells (Kanda et al., 2008; Takeda et al., 2016) (**Fig. 4D**). Unfortunately, functional studies on *LPAR6* are hampered by the lack of specific antagonists. From these results, we conclude that TIL repulsion is mediated by *LPAR6*, without excluding possible additional anti-migratory roles for its non-EDG family members *LPAR4* and *LPAR5*.

ATX secretion by tumor cells reduces CD8⁺ T-cell infiltration. We next examined whether tumor cell-secreted ATX counteracts CD8⁺ T-cell infiltration *in vivo*. For this, we turned to an anti-cancer vaccination tumor model using subcutaneous (s.c.) implanted TC-1 tumor cells that express a CD8 tumor antigen derived from the HPV16 E7 oncogene (Lin et al., 1996). These tumors are poorly immunogenic and show no spontaneous T cell infiltration. However, robust and tumor-specific CD8⁺ T cell infiltration is induced by vaccination with specific plasmid DNA (Ahrends et al., 2016; Ahrends et al., 2017). This DNA vaccine encodes HPV E7 in a gene shuffled configuration, which provides a strong MHC class I-restricted CD8 T cell epitope and MHC class II-restricted epitopes that elicit CD4⁺ T cell help. The “helped” tumor-specific CD8⁺ T cells generated upon vaccination are highly cytotoxic and display a strong migration and tumor-infiltrating capacity, partly attributable to upregulation of chemokine receptors (Ahrends et al., 2017).

Since TC-1 cells lack ATX expression, we generated ATX-expressing TC-1-ATX cells and confirmed that they secrete enzymatically active ATX (**Fig. 5A,B**). Tumor growth was comparable between TC-1- and TC-1-ATX-transplanted syngeneic mice, but there was a trend to accelerated growth of ATX-expressing TC-1 tumors (**Suppl. Fig. S3A,B**). This is in line with previous findings that ATX-LPAR signaling does not strongly promote the growth of implanted tumor cells, but rather enhances their metastatic spread through *LPAR1* (David et al., 2010; Lee et al., 2015; Marshall et al., 2012). We next vaccinated a cohort of TC-1 and TC-1-ATX tumor-bearing mice on days 8, 11 and 14 after tumor

implantation, as illustrated in **Fig. 5C**. After vaccination, T cells are primed in the vaccine-draining lymph node from where they egress into the circulation and ultimately migrate to the tumor effector site. In this model, the quantity and quality of T cells that appear in circulation reflect T cell responses in the draining lymph nodes (Ahrends et al., 2017).

We first examined whether ATX expression in TC-1 tumor cells affected the capacity of this DNA vaccine to induce a CD8⁺ T cell response, by examining the frequency of antigen-specific, tetramer-positive CD8⁺ T cells in the blood. The CD8⁺ T cell response induced by vaccination was similar between TC-1- and TC-1-ATX tumor-bearing mice (**Suppl. Fig. S3C**), indicating that ATX secretion does not affect the induction of a CD8⁺ T cell response following vaccination.

We then examined CD8⁺ T cell infiltration into ATX-secreting versus ATX-deficient tumors (on day 10 after vaccination) using immunohistochemistry. As shown in **Fig. 5D,E**, T-cell infiltration was significantly reduced in ATX-secreting tumors when compared to ATX-deficient tumors. A similar effect was observed when quantifying the frequency of tumor-specific T cells with an activated (CD43⁺) phenotype by flow cytometry (**Fig. 5F**). However, reduced T-cell infiltration did not lead to detectable effects on tumor control, as tumors in both animal groups were initially reduced, but thereafter lapsed (**Fig. 5G**). This suggests that the vaccination-induced immune response in this model is too robust to uncover effects of secreted ATX on anti-tumor responses. Hence, alternative tumor models will be needed to assess how ATX-driven reduction in TILs correlates with anti-tumor efficacy. In conclusion, these results provide proof-of-concept that ATX secreted by tumor cells opposes CD8⁺ T cell infiltration *in vivo*.

***ENPP2* expression in melanoma is associated with reduced CD8⁺ T-cell infiltration.**

Since microenvironments of s.c. engrafted tumors in mice differ considerably from those in human tumors, we sought clinical evidence for ATX functioning as a T-cell repellent in melanoma. Accordingly, we analyzed *ENPP2* expression patterns and CD8⁺ T-cell infiltration using single-cell RNA-seq results from 32 melanoma tumors (prior to immunotherapy), in which diverse cell subsets could be distinguished (Jerby-Arnon et al., 2018). *ENPP2* expression in individual cells (n=7186) and its association with cytotoxic T-cell infiltration was examined in all subsets, notably malignant cells, CD8⁺ and CD4⁺ T cells, B cells, NK cells, as well as cancer-associated fibroblasts (CAFs), macrophages and endothelial cells. **Fig. 6A** shows the melanoma samples grouped by individual cell types. Significant *ENPP2* expression was detected in malignant cells, CAFs, macrophages and endothelial cells (**Fig. 6B**). Melanoma-associated endothelial cells are likely derived from HEV-like endothelium that serves as a major gateway for TILs. Tumors with highest *ENPP2* expression overall – in both melanoma and stromal cells - contained significantly fewer CD8⁺ T cells, whereas low *ENPP2* expression was associated with enhanced CD8⁺ T cell infiltration. The negative correlation between *ENPP2* expression

and intratumoral CD8⁺ T-cell accumulation ($r=0.4$; $p=0.01$) is shown in **Fig. 6C**. While we acknowledge that single-cell RNA-seq studies do not detect all transcripts in every single cell, and the sample size ($n=32$) is not very large, these single-cell results are consistent with the above *in vivo* data, namely that intratumoral ATX opposes CD8⁺ T-cell infiltration.

Discussion

Our understanding of the factors that regulate tumor infiltration of CD8⁺ T cells is incomplete, impeding progress in improving immunotherapy efficacy. Chemokines and their GPCRs have long been in the spotlight as major drivers of T-cell attraction and trafficking; however, chemokines can also promote metastasis thus acting as two-edged swords in tumor microenvironments (Do et al., 2020). Diffusible factors that counteract T-cell attraction (“inhibitory chemokines”) have remained understudied to date. Here we reveal an unexpected role for ATX/LPA in opposing T-cell attraction both *ex vivo* and *in vivo*. Through LPAR6, ATX is the major T-cell repellent secreted by melanoma cells. This results comes as a surprise since ATX is widely known as an “autocrine” migration-stimulatory factor (Mills and Moolenaar, 2003; Perrakis and Moolenaar, 2014; Stracke et al., 1992). To the best of our knowledge, this is the first identification of a T-cell repulsive enzyme secreted by melanoma cells.

Collectively, our results support a model of the melanoma microenvironment in which ATX - secreted by both malignant and stromal cells, and in complex with LPA - counteracts T-cell infiltration via LPAR6 while it activates melanoma cells and cancer-associated fibroblasts via LPAR1 (**Fig. 6D**). Hence, the ATX:LPA complex exerts opposite but complementary actions in the tumor immune microenvironment via different LPA receptors. Since ATX is abundantly expressed in most solid tumors (**Suppl. Fig. S1B**), this model extends beyond melanoma. Of note, in common with actin-remodeling GPCR agonists, LPA evoked an immediate-early gene expression signature in TILs (**Suppl. Fig. 2A,B**), the underpinnings and physiological consequences of which deserve further investigation.

Tumor microenvironments are very heterogeneous and cancer type-specific, implying that ATX/LPA signaling outcome will critically depend on the composition and LPAR expression repertoire of the immune cell infiltrate. LPAR6 is of special interest here as it provides a crucial link with ATX and $G\alpha_{13}$ during embryonic development (van Meeteren et al., 2006; Yasuda et al., 2019) and is abundantly expressed in immune cells (**Figure 3D**). LPAR6 has a rather low affinity for 1-acyl-LPA species (Yung et al., 2014), which may explain the relatively high IC_{50} value for 1-oleyl-LPA observed in the T-cell migration assays (**Fig. 1B**). Interestingly, LPAR6 (then 6H1) is strongly upregulated upon activation of chicken T cells (Kaplan et al., 1993) and modestly downregulated (approx. 1.8-fold) in “helped” CD8⁺ T cells, along with PD-1 and other co-inhibitory receptors (Ahrends et al.,

2017) (T. Ahrends, J. Borst, unpublished results). This defines LPAR6 as an inducible receptor whose regulation is currently unknown. Although LPAR4 and LPAR5 were not expressed in *ex vivo* expanded TILs, the latter receptor is nonetheless of immunological importance since its genetic deletion in mice enhances T-cell receptor activity and anti-tumor responses (Mathew et al., 2019). Studies using *Lpar5^{-/-}/Lpar6^{-/-}* double-knockout mice should aid to elucidate the combined actions of these non-EDG LPA receptors on T-cell migratory behavior and anti-tumor efficacy.

Importantly and contrary to prevailing notions, we find that secreted ATX is fully bioactive at physiologically insignificant (“near-zero”) extracellular LPA levels. ATX thus emerges as a “dual-function” protein that both produces and chaperones LPA by virtue the fact that it binds and protects LPA in its “tunnel” for efficient delivery to its GPCRs when ATX binds to the cell surface via integrins or heparan sulfate proteoglycans (Fulkerson et al., 2011; Hausmann et al., 2011; Houben et al., 2013; Kanda et al., 2008). The calculated lifetime of the ATX/LPA complex is relatively long (Salgado-Polo et al., 2018; Saunders et al., 2011), allowing ATX-bound LPA to diffuse over a relatively long distance in cellular environments. Precisely how ATX delivers bound LPA to its receptors awaits further structural and functional studies.

On a final note, while the present findings leave several new questions unanswered, our study paves the way for addressing outstanding questions in other immunotherapeutic settings, notably melanoma PDX models to be re-infused with patient-derived autologous TILs. Such clinically relevant models should allow us to assess how ATX-dependent TIL exclusion correlates with anti-tumor efficacy in a defined context, and above all, to evaluate the anti-tumor benefits of pharmacological ATX inhibition, conceivably in combination with immune checkpoint inhibitors.

Methods

Cell culture and materials. MDA-MB-435 and A375M melanoma cells were grown in Dulbecco’s modified Eagle’s medium (DMEM) supplemented with 10% fetal bovine serum (FBS) at 37°C under 5% CO₂. Patient-derived TILs cells were grown in Roswell Park Memorial Institute (RPMI) 1640 Medium supplemented with 10% human serum at 37°C under 5% CO₂. Human CD8⁺ T cells were isolated from buffy coats, activated with anti-CD3 and CD28 mAbs that were plate-bound and expanded in RPMI 1640 Medium supplemented with 10% human serum and 100 IU/mL interleukin-2 and 5 ng/mL interleukin-15 at 37°C under 5% CO₂. Interleukins and CXCL10 were from PeproTech. LPA(1-oleoyl) was obtained from Avanti Polar Lipids. Human ATX was produced in HEK293 Flip-in cells and purified as previously described (Salgado-Polo et al., 2018). Fibronectin and PF-8380 were purchased from Sigma-Aldrich. IOA-289 (formerly CRT750) was synthesized as previously described (Shah et al., 2016).

Isolation and expansion of melanoma-derived TILs. TIL isolation and expansion was started by generation of a single cell suspension by enzymatic digestion of the resected metastatic tumor material obtained by surgery. Resulting cell suspensions were cultured in the presence of 6000 IU/ml IL-2 (Proleukin, Novartis) for two to four weeks. During the subsequent Rapid Expansion Protocol (REP) of two weeks, T cells were cultured in 50% RPMI/50% AIM-V medium in the presence of 3,000 IU/ml IL-2, 30 ng/ml anti-CD3 (OKT-3, Miltenyi) and irradiated autologous PBMCs (feeder cells in 200-fold excess over TIL).

Isolation of peripheral CD8⁺ T cells. Human peripheral blood mononuclear cells (PBMCs) were isolated from fresh buffy coats using Ficoll-Paque Plus (GE Healthcare) gradient centrifugation. Total CD8⁺T cells were isolated using magnetic sorting with CD8 microbeads (Miltenyi Biotec). Blood samples were obtained from anonymized healthy male donors with written informed consent in accordance to guidelines established by the Sanquin Medical Ethical Committee.

Conditioned media. Conditioned media were collected from MDA-MB435 and A375M cells. Sub-confluent 10-cm dishes of melanoma cells were washed with PBS and incubated in serum-free DMEM. Conditioned medium was harvested after 24 and 48 hrs, and centrifuged for 30 min at 4000 rpm to remove cell debris.

Transwell migration assays. T cell migration was measured using 48-well chemotaxis chambers (Neuro Probe, Inc.) equipped with 5 µm-pore polycarbonate membranes (8 µm-pore for melanoma cells), which were coated with fibronectin (1 µg/ml). Cells (1×10⁶/ml) were added to the upper chamber. Fatty acid-free BSA (1 mg/ml) was used as a lysophospholipid carrier. Migration was allowed for 2 hrs for TILs and CD8⁺ T cells, and 4 hrs for melanoma cells, at 37°C in humidified air containing 5% CO₂. Migrated cells were fixed in Diff-Quik Fix and stained using Diff-Quik II. Migration was quantified by color intensity measurements using Image J software.

ATX lysoPLD activity. ATX enzymatic activity in conditioned media was measured by steady-state choline release from exogenously added LPC using a coupled reaction, as detailed elsewhere (Salgado-Polo et al., 2018). Briefly, media were centrifuged for 45 min at 4,500 rpm, upon which 75 µl of the supernatants were plated on 96-well plates together with 600 µM LPC(18:1), 1 U ml⁻¹ choline oxidase, 2 U ml⁻¹ horseradish peroxidase (HRP) and 2 mM homovanillic acid (HVA), reaching a final volume of 100 µl. ATX activity was measured by HVA fluorescence at $\lambda_{ex}/\lambda_{em} = 320/460$ nm every 30 s for at least 160 min at 37°C with a Pherastar plate reader (BMG Labtech). Since ATX activity *in vitro* presents a ~15-min lag phase, the subsequent linear slope (60-160 min) was used to perform all analyses. Triplicate measures were statistically analyzed by unpaired t test.

Western blotting. Cells were washed in ice-cold PBS (phosphate-buffered saline containing 2 mM Ca₂⁺ and Mg₂⁺), lysed in RIPA buffer with protease inhibitors and spun down. Equal amounts of proteins were determined by BCA protein assay kit (Pierce), separated by SDS-PAGE using pre-cast gradient gels (4-12% Nu-Page Bis-Tris, Invitrogen) and transferred to nitrocellulose membranes. The membrane was blocked for 1 hour at room-temperature in 5% skimmed milk in TBST. Incubation with antibodies was done overnight at 4°C, followed by 1 hr incubation with horseradish peroxidase-conjugated secondary antibodies (DAKO, Glostrup, Denmark). Proteins were visualized using ECL Western blot reagent (GE Healthcare, Chalfont St. Giles, UK).

qPCR analysis. Expression levels of LPA receptors and ATX/ENPP2 were quantified by RT-qPCR. Total RNA was isolated using GeneJET purification kit (Fermentas). cDNA was synthesized by reverse transcription from 2 mg RNA with oligodT 15 primers and SSII RT enzyme (Invitrogen). qPCR was performed on a 7500 Fast System (Applied Biosystems) as follows: 95°C for 2 min followed by 40 cycles at 95°C for 15 s followed by 60°C for 1 min. 200 nM forward and reverse primers, 16 ml SYBR Green Supermix (Applied Biosystems) and diluted cDNA were used in the final reaction mixture. Cyclophilin was used as reference gene and milliQ was used as negative control. Normalized expression was calculated following the equation $NE = 2^{-(Ct\ target - Ct\ reference)}$. Primers used: LPA1 forward AATCGGGATACCATGATGAGT, reverse CCAGGAGTCCAGCAGATGATAAA; LPA2 forward CGCTCAGCCTGGTCAAAGACT, reverse TTGCAGGACTCACAGCCTAAAC; LPA3 forward AGGACACCCATGAAGCTAATGAA, reverse GCCGTCGAGGAGCAGAAC; LPA4 forward CCTAGTCCTCAGTGGCGGTATT, reverse CCTTCAAAGCAGGTGGTGGTT; LPA5 forward CCAGCGACCTGCTCTTCAC, reverse CCAGTGGTGCAGTGCGTAGT; LPA6 forward AACTGGTCTGTTCAGGAGAAGT, reverse CAGGCAGCAGATTCATTGTCA; ENPP2 forward ATTACAGCCACCAAGCAAGG, reverse TCCCTCAGAGGATTTGTCAT; β -actin forward GCTCTTTCCAGCCTTCCTT, reverse CTTCTGCATCCTGTCAGCAA; Cyclophilin forward CATCTGCACTGCCAAGACTGA and reverse TTGCCAAACACCATGCTT.

ATX knockdown. For ATX knockdown studies, we used five human ENPP2 shRNAs in the lentiviral vector pLKO1: (TRC human shRNA library; TRCN0000048993, TRCN0000048995-TRCN0000048997 and TRCN0000174091). To generate particles for stable infections, HEK293T cells were transfected with single shRNA hairpins using the calcium phosphate protocol; the virus particles were collected at 48 hrs after transfection. ENPP2 stable knockdown cells were selected and maintained in medium containing 2 μ g/ml puromycin.

Lipid extraction and LC-MS/MS measurements of LPA. Extraction of lipids from cell-free conditioned media was done using acidified organic solvents and measurement of seventeen LPA species was accomplished using LC-MS/MS. Quantitation of LPA species was achieved using LPA(17:0) as an internal standard. Experimental details can be found elsewhere (Kraemer et al., 2019).

RNA sequencing and bioinformatics of LPA-treated TILs. RNA from melanoma TILs before and after LPA treatment (2 and 3 hrs) was extracted and subjected to RNA sequencing (RNAseq) at the NKI Genomics Core Facility. The samples were sequenced on a Illumina HiSeq-2500 machine. The sequencing reads with a length of 65 basepairs are mapped to the human reference genome (hg38) using TopHat (version 2.0.12) TopHat was supplied with a known set of gene models (Gene Transfer File Ensembl version 77). In order to determine the number of reads per gene, a custom script (Itreecount) was used, based on the HTSeq-count. Itreecount generates a list of the total number of uniquely mapped sequencing reads for each gene that is present in the provided GTF file. Differential expression was performed on normalized and library size corrected counts using the R package Limma/Voom. Resulting p-values are corrected for multiple testing. A gene was considered differentially expressed if the p-value <0.05. Raw sequence data are deposited at GEO (accession number GSE143697).

TILs phenotypes and autologous tumor recognition. TILs were phenotypically characterized by flow cytometry with or without addition of LPA using antibodies directed against the indicated T-cell markers. Cells were analyzed on a FACS LSR2 SORP (BD) machine and data were processed using Flowjo_V10 software. To detect IFN- γ production, 2×10^5 TILs were cultured with 2×10^5 cells

from tumor digest or tumor cell lines, in the presence of 1 μ /ml Golgiplug (BD Biosciences), with or without the addition of LPA. After 5 hrs, cells were stained using anti-CD8 antibody (clone SKI, BD bioscience) and live/dead marker (Fixable Violet Dead cells stain Kit, (Invitrogen)). Production of cytokine IFN- γ was detected after cell fixation and permeabilization with a Cytotfix/Cytoperm kit (BD) and antibody against cytokine IFN- γ (clone B27) from BD Bioscience.

Studies in mice. Six to eight-week old female C57BL/6JRj (B6) mice were obtained from Janvier Laboratories (Le Genest Saint Isle, France) and maintained in individually ventilated cages (Innovive, San Diego, CA) under specific pathogen-free conditions. All mouse experiments were performed in accordance with institutional and national guidelines and were approved by the Committee for Animal Experimentation at the NKI.

Tumor cells and transplantation. TC-1 tumor cells are derived from lung epithelial cells that express HPV16 E6 and E7 proteins. Cells were obtained from the Leiden University Medical Center in 2015, and further authentication was not performed by the authors. TC-1 cells stably overexpressing ATX were generated by retroviral transduction and ATX overexpression was validated by Western Blotting. TC-1 cells were cultured in RPMI1640, supplemented with 10% fetal calf serum (FCS), 0.1 mM non-essential amino acids, 1 mM sodium pyruvate, 2 mM L-glutamine, 10 mM HEPES, penicillin, streptomycin and primocin at 37°C, 5% CO₂. TC-1 cells were tested negative for *Mycoplasma* by PCR, and cells thawed from this 'master stock' were routinely used within 6 passages (approximately 3 weeks) for *in vitro* and *in vivo* experiments. On day 0, mice were anesthetized with isoflurane and injected s.c. with $\sim 2 \times 10^5$ TC-1 tumor cells. Vaccination was performed on day 8 after inoculation and mice were treated with 10 μ l/kg 1% methylcellulose twice weekly. Tumor size was measured by caliper in two dimensions and calculated as: area (mm²) = (width x length). Mice were monitored two times per week. Mice were sacrificed when the tumor diameter reached 15 mm or when the tumor size reached 100-200mm². A tumor size of 100 mm² was set as a designated end point.

Vaccination. Generation and validation of the HELP-E7SH DNA vaccines and the amino acid sequences encoded by them were designed as described and detailed previously (Ahrends et al., 2016). Intra-epidermal DNA "tattoo" vaccination was performed as described (Ahrends et al., 2017). Briefly, the hair on a hind leg was removed using depilating cream (Veet, Reckitt Benckiser) on day 8 (after tumor implantation). On days 8, 11, and 14 after tumor implantation, mice were anesthetized and 15 μ L of a solution containing 2 mg/ml plasmid DNA in 10 mM Tris and 1 mM EDTA, pH 8.0 was applied to the hairless skin with a Permanent Make Up tattoo machine (MT Derm GmbH, Berlin, Germany), using a sterile disposable 9-needle bar with a needle depth of 1 mm and oscillating at a frequency of 100 Hz for 45 sec.

Tissue preparation and flow cytometry. Tissue preparation and flow cytometry was performed essentially as follows. On day 18 after tumor implantation (day 10 after start of vaccination), mice were sacrificed and tumor and lymphoid tissue were harvested. The tumors were mechanically chopped using a McIlwain tissue chopper (Mickle Laboratory Engineering), and a single-cell suspension was prepared by digesting the tissue in collagenase type A (Roche) and 25 μ g/ml DNase (Sigma) in serum-free DMEM medium for 45 min at 37°C. Enzyme activity was neutralized by addition of DMEM containing 8% FCS, and the tissue was dispersed by passing through a 70- μ m cell strainer. A single-cell suspension of lymphoid tissue was prepared by passing the tissue through a 70- μ m cell strainer. Single cells were first stained with APC-conjugated H-2D_b E7₅₉₋₅₇ (RAHYNIVTF) tetramers (Tetramer Facility, Leiden University Medical Center) for 15 min at 4°C in the dark. After tetramer staining, tumor cells were blocked with 2% mouse serum (NMS) with DNase (10 μ g/ml) for 15 minutes on ice. For surface staining, cells were incubated with

fluorochrome conjugated antibodies (see below), and 0.5 ul anti-APC (clone APC003, BioLegend) per sample to increase intensity of tetramer staining, for 30 minutes on ice in the dark in PBS containing 0.5% BSA and 0.01% sodium azide. LIVE/DEAD™ Fixable Near-IR Dead Cell Stain Kit (1:1000, Invitrogen) was added to exclude dead cells. All experiments were analyzed using a BD Symphony A5 flow cytometer with Diva software, and the generated data were analyzed using FlowJo software. Fluorochrome-conjugated mAbs with the following specificities were used for flow cytometry and obtained from BD Pharmingen (Breda, the Netherlands) unless otherwise specified: CD8-eFluor450 (1:200, clone 56-6.7), CD4-BV711 (1:200, clone GK1.5), TCRβ-PECy7 (1:100; clone H57-597), CD43-PerCPCy5.5 (1:200, clone 1B11 (BioLegend, San Diego, CA)), CD45-2-BUV395 (1:200; clone 30-F11).

Immunohistochemical analysis. Harvested tumors were fixed for 24 hrs in ethanol (50%), acetic acid (5%) and formalin (3.7%), embedded in paraffin, and then sectioned randomly at 5 mm. The sections were then stained as follows. Fixed sections were rehydrated and then incubated with primary antibodies to CD8 (eBioscience; clone 4SM15). Endogenous peroxidases were blocked with 3% H₂O₂, and the sections were then incubated with biotin-conjugated secondary antibodies, followed by incubation with HRP-conjugated streptavidin-biotin (DAKO). The substrate was developed using diaminobenzidine (DAB) (DAKO). We included negative controls to determine background staining, which was negligible. The stained sections were digitally processed using an Aperio ScanScope (Aperio, Vista, CA) equipped with a 20x objective. ImageJ software was used to quantify the number of positive cells in 8 random fields of view (FOV) per slide. Images were analyzed with a custom-made macro for ImageJ by counting the cells above a pre-defined CD8-intensity threshold.

Single-cell RNA-seq analysis of human melanoma tumors. Single-cell data from 32 melanoma tumors (Jerby-Arnon et al., 2018) was downloaded from NCBI GEO ([gse115978](https://www.ncbi.nlm.nih.gov/geo/query/acc.cgi?acc=gse115978)) and exported to the R2 platform (<http://r2.amc.nl>, Mixed Melanoma SC - Regev - 7186 - tpm - gse115978). tSNE clustering was applied to 7186 cells. A perplexity of 5 was chosen to represent the cohort. Inferred cell type information was extracted from the GEO dataset. Expression of ENPP2 and other annotations were projected onto the tSNE embedding. In every patient sample, the percentage of ENPP2-expressing cells was correlated to the percentage of cells inferred to be CD8⁺-positive. All analyses of the single-cell data were performed in the R2 genomics analysis and visualization platform.

Statistical analysis. For in vitro migration assays, a two-tailed unpaired Student's t-test was applied. A P value < 0.05 was considered statistically significant; *, p < 0.05; **, P < 0.005; ***, P < 0.001; and ****, P < 0.0001. Data from mouse studies were analyzed for homogeneity of variance between groups by Levene's test. Effect of ATX expression on T-cell infiltration was analyzed by a Generalized Linear Model using gamma distribution and log as link factor. Nested factor was included in the model in order to study the variation between mice. FACS experiments were analyzed by Generalized Linear Model using gamma distribution and log link factor. Analysis were performed using IBM SPSS Statistics v. 25.

Accession numbers - Primary RNA-seq data are deposited at GEO, accession number GSE143697.

Acknowledgements - We thank Paula Voabil, Jos Urbanus, Yanling Xao and Elselien Frijlink for help with immunological experiments and data analysis, and Tomasz Ahrends and Anne van der Leun for helpful discussions and sharing unpublished data. This work was supported by private

funding to W.H.M and grants from the Dutch Cancer Society (grants NKI 2013-5951 and 10764 to I.V.); NWO-STW (J.M.A), and P30 GM127211 from the NIH to A.J.M.

Author contributions - E.M.-R.: conceptualization, investigation, analysis, methodology, validation, visualization and writing; I.v.d.H.A.: investigation, methodology, analysis, validation, and visualization; M.v.Z.: investigation, methodology, analysis, validation, and visualization; A.J.M.: investigation, methodology, and analysis; J.K.: investigation, methodology, analysis, and visualization; F.S.-P.: investigation, methodology, analysis, and visualization; I.d.R.: investigation, methodology, analysis, and visualization; S.K.: methodology and analysis; T.L.: methodology and analysis; J.H.: conceptualization and methodology; J.M.A: methodology and analysis; Z.J.: conceptualization, analysis, and methodology; S.F.: conceptualization and methodology; T.N.S.: conceptualization, methodology; A.P.: analysis, methodology, and validation; J.B.: conceptualization, analysis, methodology; I.V.: conceptualization, investigation, analysis, methodology, validation, visualization, and writing; J.v.d.B.: conceptualization, investigation, analysis, methodology, and validation; W.H.M.: conceptualization, analysis, methodology, validation, supervision, and writing.

References

- Ahrends, T., Babala, N., Xiao, Y., Yagita, H., van Eenennaam, H., and Borst, J. (2016). CD27 Agonism Plus PD-1 Blockade Recapitulates CD4+ T-cell Help in Therapeutic Anticancer Vaccination. *Cancer research* *76*, 2921-2931.
- Ahrends, T., Spanjaard, A., Pilzecker, B., Babala, N., Bovens, A., Xiao, Y., Jacobs, H., and Borst, J. (2017). CD4(+) T Cell Help Confers a Cytotoxic T Cell Effector Program Including Coinhibitory Receptor Downregulation and Increased Tissue Invasiveness. *Immunity* *47*, 848-861 e845.
- Anandappa, A. J., Wu, C. J., and Ott, P. A. (2020). Directing Traffic: How to Effectively Drive T Cells into Tumors. *Cancer discovery*.
- Auciello, F. R., Bulusu, V., Oon, C., Tait-Mulder, J., Berry, M., Bhattacharyya, S., Tumanov, S., Allen-Petersen, B. L., Link, J., Kendersky, N. D., *et al.* (2019). A Stromal Lysolipid-Autotaxin Signaling Axis Promotes Pancreatic Tumor Progression. *Cancer discovery* *9*, 617-627.
- Bai, Z., Cai, L., Umemoto, E., Takeda, A., Tohya, K., Komai, Y., Veeraveedu, P. T., Hata, E., Sugiura, Y., Kubo, A., *et al.* (2013). Constitutive lymphocyte transmigration across the basal lamina of high endothelial venules is regulated by the autotaxin/lysophosphatidic acid axis. *Journal of immunology* *190*, 2036-2048.
- Battle, E., and Massague, J. (2019). Transforming Growth Factor-beta Signaling in Immunity and Cancer. *Immunity* *50*, 924-940.
- Benesch, M. G. K., MacIntyre, I. T. K., McMullen, T. P. W., and Brindley, D. N. (2018). Coming of Age for Autotaxin and Lysophosphatidate Signaling: Clinical Applications for Preventing, Detecting and Targeting Tumor-Promoting Inflammation. *Cancers (Basel)* *10*.

Chen, D. S., and Mellman, I. (2013). Oncology meets immunology: the cancer-immunity cycle. *Immunity* 39, 1-10.

Choi, J. W., Herr, D. R., Noguchi, K., Yung, Y. C., Lee, C. W., Mutoh, T., Lin, M. E., Teo, S. T., Park, K. E., Mosley, A. N., and Chun, J. (2010). LPA receptors: subtypes and biological actions. *Annual review of pharmacology and toxicology* 50, 157-186.

Chow, M. T., and Luster, A. D. (2014). Chemokines in cancer. *Cancer immunology research* 2, 1125-1131.

David, M., Wannecq, E., Descotes, F., Jansen, S., Deux, B., Ribeiro, J., Serre, C. M., Gres, S., Bendriss-Vermare, N., Bollen, M., *et al.* (2010). Cancer cell expression of autotaxin controls bone metastasis formation in mouse through lysophosphatidic acid-dependent activation of osteoclasts. *PLoS One* 5, e9741.

Do, H. T. T., Lee, C. H., and Cho, J. (2020). Chemokines and their Receptors: Multifaceted Roles in Cancer Progression and Potential Value as Cancer Prognostic Markers. *Cancers (Basel)* 12.

Esnault, C., Stewart, A., Gualdrini, F., East, P., Horswell, S., Matthews, N., and Treisman, R. (2014). Rho-actin signaling to the MRTF coactivators dominates the immediate transcriptional response to serum in fibroblasts. *Genes & development* 28, 943-958.

Filipp, F. V., Li, C., and Boiko, A. D. (2019). CD271 is a molecular switch with divergent roles in melanoma and melanocyte development. *Scientific reports* 9, 7696.

Fridman, W. H., Zitvogel, L., Sautes-Fridman, C., and Kroemer, G. (2017). The immune contexture in cancer prognosis and treatment. *Nature reviews Clinical oncology* 14, 717-734.

Fulkerson, Z., Wu, T., Sunkara, M., Kooi, C. V., Morris, A. J., and Smyth, S. S. (2011). Binding of autotaxin to integrins localizes lysophosphatidic acid production to platelets and mammalian cells. *J Biol Chem* 286, 34654-34663.

Ghandi, M., Huang, F. W., Jane-Valbuena, J., Kryukov, G. V., Lo, C. C., McDonald, E. R., 3rd, Barretina, J., Gelfand, E. T., Bielski, C. M., Li, H., *et al.* (2019). Next-generation characterization of the Cancer Cell Line Encyclopedia. *Nature* 569, 503-508.

Gierse, J., Thorarensen, A., Beltey, K., Bradshaw-Pierce, E., Cortes-Burgos, L., Hall, T., Johnston, A., Murphy, M., Nemirovskiy, O., Ogawa, S., *et al.* (2010). A novel autotaxin inhibitor reduces lysophosphatidic acid levels in plasma and the site of inflammation. *The Journal of pharmacology and experimental therapeutics* 334, 310-317.

Giraldo, N. A., Sanchez-Salas, R., Peske, J. D., Vano, Y., Becht, E., Petitprez, F., Validire, P., Ingels, A., Cathelineau, X., Fridman, W. H., and Sautes-Fridman, C. (2019). The clinical role of the TME in solid cancer. *British journal of cancer* 120, 45-53.

Hausmann, J., Kamtekar, S., Christodoulou, E., Day, J. E., Wu, T., Fulkerson, Z., Albers, H. M., van Meeteren, L. A., Houben, A. J., van Zeijl, L., *et al.* (2011). Structural basis of substrate discrimination and integrin binding by autotaxin. *Nature structural & molecular biology* 18, 198-204.

Hinshaw, D. C., and Shevde, L. A. (2019). The Tumor Microenvironment Innately Modulates Cancer Progression. *Cancer research* 79, 4557-4566.

Hisano, Y., and Hla, T. (2019). Bioactive lysolipids in cancer and angiogenesis. *Pharmacology & therapeutics* 193, 91-98.

Houben, A. J., van Wijk, X. M., van Meeteren, L. A., van Zeijl, L., van de Westerlo, E. M., Hausmann, J., Fish, A., Perrakis, A., van Kuppevelt, T. H., and Moolenaar, W. H. (2013). The polybasic insertion in autotaxin alpha confers specific binding to heparin and cell surface heparan sulfate proteoglycans. *J Biol Chem* 288, 510-519.

Inoue, A., Raimondi, F., Kadji, F. M. N., Singh, G., Kishi, T., Uwamizu, A., Ono, Y., Shinjo, Y., Ishida, S., Arang, N., *et al.* (2019). Illuminating G-Protein-Coupling Selectivity of GPCRs. *Cell* 177, 1933-1947 e1925.

Jerby-Arnon, L., Shah, P., Cuoco, M. S., Rodman, C., Su, M. J., Melms, J. C., Leeson, R., Kanodia, A., Mei, S., Lin, J. R., *et al.* (2018). A Cancer Cell Program Promotes T Cell Exclusion and Resistance to Checkpoint Blockade. *Cell* 175, 984-997 e924.

Jongsma, M., Matas-Rico, E., Rzadkowski, A., Jalink, K., and Moolenaar, W. H. (2011). LPA is a chemorepellent for B16 melanoma cells: action through the cAMP-elevating LPA5 receptor. *PLoS One* 6, e29260.

Kanda, H., Newton, R., Klein, R., Morita, Y., Gunn, M. D., and Rosen, S. D. (2008). Autotaxin, an ectoenzyme that produces lysophosphatidic acid, promotes the entry of lymphocytes into secondary lymphoid organs. *Nature immunology* 9, 415-423.

Kaplan, M. H., Smith, D. I., and Sundick, R. S. (1993). Identification of a G protein coupled receptor induced in activated T cells. *Journal of immunology* 151, 628-636.

Kerdidani, D., Chouvardas, P., Arjo, A. R., Giopanou, I., Ntaliarda, G., Guo, Y. A., Tsikitis, M., Kazamias, G., Potaris, K., Stathopoulos, G. T., *et al.* (2019). Wnt1 silences chemokine genes in dendritic cells and induces adaptive immune resistance in lung adenocarcinoma. *Nature communications* 10, 1405.

Keune, W. J., Hausmann, J., Bolier, R., Tolenaars, D., Kremer, A., Heidebrecht, T., Joosten, R. P., Sunkara, M., Morris, A. J., Matas-Rico, E., *et al.* (2016). Steroid binding to Autotaxin links bile salts and lysophosphatidic acid signalling. *Nature communications* 7, 11248.

Knowlden, S. A., Capece, T., Popovic, M., Chapman, T. J., Rezaee, F., Kim, M., and Georas, S. N. (2014). Regulation of T cell motility in vitro and in vivo by LPA and LPA2. *PLoS One* 9, e101655.

Kraemer, M., Mao, G., Hammill, C., Yan, B., Li, Y., Onono, F., Smyth, S. S., and Morris, A. J. (2019). Effects of diet and hyperlipidemia on levels and distribution of circulating lysophosphatidic acid. *Journal of lipid research*.

Lee, S. C., Fujiwara, Y., Liu, J., Yue, J., Shimizu, Y., Norman, D. D., Wang, Y., Tsukahara, R., Szabo, E., Patil, R., *et al.* (2015). Autotaxin and LPA1 and LPA5 receptors exert disparate functions in tumor cells versus the host tissue microenvironment in melanoma invasion and metastasis. *Molecular cancer research : MCR* 13, 174-185.

Lee, Z., Cheng, C. T., Zhang, H., Subler, M. A., Wu, J., Mukherjee, A., Windle, J. J., Chen, C. K., and Fang, X. (2008). Role of LPA4/p2y9/GPR23 in negative regulation of cell motility. *Mol Biol Cell* 19, 5435-5445.

Li, H., van der Leun, A. M., Yofe, I., Lubling, Y., Gelbard-Solodkin, D., van Akkooi, A. C. J., van den Braber, M., Rozeman, E. A., Haanen, J., Blank, C. U., *et al.* (2019). Dysfunctional CD8 T Cells Form a Proliferative, Dynamically Regulated Compartment within Human Melanoma. *Cell* *176*, 775-789 e718.

Lin, K. Y., Guarnieri, F. G., Staveley-O'Carroll, K. F., Levitsky, H. I., August, J. T., Pardoll, D. M., and Wu, T. C. (1996). Treatment of established tumors with a novel vaccine that enhances major histocompatibility class II presentation of tumor antigen. *Cancer Res* *56*, 21-26.

Lin, S., Haque, A., Raeman, R., Guo, L., He, P., Denning, T. L., El-Rayes, B., Moolenaar, W. H., and Yun, C. C. (2019). Autotaxin determines colitis severity in mice and is secreted by B cells in the colon. *FASEB journal : official publication of the Federation of American Societies for Experimental Biology* *33*, 3623-3635.

Liu, S., Umezu-Goto, M., Murph, M., Lu, Y., Liu, W., Zhang, F., Yu, S., Stephens, L. C., Cui, X., Murrow, G., *et al.* (2009). Expression of autotaxin and lysophosphatidic acid receptors increases mammary tumorigenesis, invasion, and metastases. *Cancer Cell* *15*, 539-550.

Marshall, J. C., Collins, J. W., Nakayama, J., Horak, C. E., Liewehr, D. J., Steinberg, S. M., Albaugh, M., Vidal-Vanaclocha, F., Palmieri, D., Barbier, M., *et al.* (2012). Effect of inhibition of the lysophosphatidic acid receptor 1 on metastasis and metastatic dormancy in breast cancer. *Journal of the National Cancer Institute* *104*, 1306-1319.

Mathew, D., Kremer, K. N., Strauch, P., Tigyi, G., Pelanda, R., and Torres, R. M. (2019). LPA5 Is an Inhibitory Receptor That Suppresses CD8 T-Cell Cytotoxic Function via Disruption of Early TCR Signaling. *Frontiers in immunology* *10*, 1159.

Mills, G. B., and Moolenaar, W. H. (2003). The emerging role of lysophosphatidic acid in cancer. *Nat Rev Cancer* *3*, 582-591.

Moolenaar, W. H., and Perrakis, A. (2011). Insights into autotaxin: how to produce and present a lipid mediator. *Nat Rev Mol Cell Biol* *12*, 674-679.

Nam, S. W., Clair, T., Kim, Y. S., McMarlin, A., Schiffmann, E., Liotta, L. A., and Stracke, M. L. (2001). Autotaxin (NPP-2), a metastasis-enhancing motogen, is an angiogenic factor. *Cancer research* *61*, 6938-6944.

Nishimasu, H., Okudaira, S., Hama, K., Mihara, E., Dohmae, N., Inoue, A., Ishitani, R., Takagi, J., Aoki, J., and Nureki, O. (2011). Crystal structure of autotaxin and insight into GPCR activation by lipid mediators. *Nature structural & molecular biology* *18*, 205-212.

Perrakis, A., and Moolenaar, W. H. (2014). Autotaxin: structure-function and signaling. *Journal of lipid research* *55*, 1010-1018.

Sackstein, R., Schatton, T., and Barthel, S. R. (2017). T-lymphocyte homing: an underappreciated yet critical hurdle for successful cancer immunotherapy. *Laboratory investigation; a journal of technical methods and pathology* *97*, 669-697.

Salgado-Polo, F., Fish, A., Matsoukas, M. T., Heidebrecht, T., Keune, W. J., and Perrakis, A. (2018). Lysophosphatidic acid produced by autotaxin acts as an allosteric modulator of its catalytic efficiency. *J Biol Chem* *293*, 14312-14327.

Saunders, L. P., Cao, W., Chang, W. C., Albright, R. A., Braddock, D. T., and De La Cruz, E. M. (2011). Kinetic analysis of autotaxin reveals substrate-specific catalytic pathways and a mechanism for lysophosphatidic acid distribution. *J Biol Chem* 286, 30130-30141.

Sciorra, V. A., and Morris, A. J. (2002). Roles for lipid phosphate phosphatases in regulation of cellular signaling. *Biochim Biophys Acta* 1582, 45-51.

Shah, P., Cheasty, A., Foxton, C., Raynham, T., Farooq, M., Gutierrez, I. F., Lejeune, A., Pritchard, M., Turnbull, A., Pang, L., *et al.* (2016). Discovery of potent inhibitors of the lysophospholipase autotaxin. *Bioorganic & medicinal chemistry letters* 26, 5403-5410.

Sharma, P., and Allison, J. P. (2015). The future of immune checkpoint therapy. *Science* 348, 56-61.

Spranger, S., Bao, R., and Gajewski, T. F. (2015). Melanoma-intrinsic beta-catenin signalling prevents anti-tumour immunity. *Nature* 523, 231-235.

Stortelers, C., Kerkhoven, R., and Moolenaar, W. H. (2008). Multiple actions of lysophosphatidic acid on fibroblasts revealed by transcriptional profiling. *BMC Genomics* 9, 387.

Stracke, M. L., Krutzsch, H. C., Unsworth, E. J., Arestad, A., Cioce, V., Schiffmann, E., and Liotta, L. A. (1992). Identification, purification, and partial sequence analysis of autotaxin, a novel motility-stimulating protein. *J Biol Chem* 267, 2524-2529.

Tager, A. M., LaCamera, P., Shea, B. S., Campanella, G. S., Selman, M., Zhao, Z., Polosukhin, V., Wain, J., Karimi-Shah, B. A., Kim, N. D., *et al.* (2008). The lysophosphatidic acid receptor LPA1 links pulmonary fibrosis to lung injury by mediating fibroblast recruitment and vascular leak. *Nature medicine* 14, 45-54.

Takahashi, K., Fukushima, K., Onishi, Y., Inui, K., Node, Y., Fukushima, N., Honoki, K., and Tsujiuchi, T. (2017). Lysophosphatidic acid (LPA) signaling via LPA4 and LPA6 negatively regulates cell motile activities of colon cancer cells. *Biochemical and biophysical research communications* 483, 652-657.

Takeda, A., Kobayashi, D., Aoi, K., Sasaki, N., Sugiura, Y., Igarashi, H., Tohya, K., Inoue, A., Hata, E., Akahoshi, N., *et al.* (2016). Fibroblastic reticular cell-derived lysophosphatidic acid regulates confined intranodal T-cell motility. *eLife* 5, e10561.

Thommen, D. S., and Schumacher, T. N. (2018). T Cell Dysfunction in Cancer. *Cancer Cell* 33, 547-562.

Tokumura, A., Majima, E., Kariya, Y., Tominaga, K., Kogure, K., Yasuda, K., and Fukuzawa, K. (2002). Identification of human plasma lysophospholipase D, a lysophosphatidic acid-producing enzyme, as autotaxin, a multifunctional phosphodiesterase. *J Biol Chem* 277, 39436-39442.

Umezū-Goto, M., Kishi, Y., Taira, A., Hama, K., Dohmae, N., Takio, K., Yamori, T., Mills, G. B., Inoue, K., Aoki, J., and Arai, H. (2002). Autotaxin has lysophospholipase D activity leading to tumor cell growth and motility by lysophosphatidic acid production. *J Cell Biol* 158, 227-233.

van der Woude, L. L., Gorris, M. A. J., Halilovic, A., Figdor, C. G., and de Vries, I. J. M. (2017). Migrating into the Tumor: a Roadmap for T Cells. *Trends Cancer* 3, 797-808.

van Meeteren, L. A., Ruurs, P., Stortelers, C., Bouwman, P., van Rooijen, M. A., Pradere, J. P., Pettit, T. R., Wakelam, M. J., Saulnier-Blache, J. S., Mummery, C. L., *et al.* (2006). Autotaxin, a secreted lysophospholipase D, is essential for blood vessel formation during development. *Mol Cell Biol* 26, 5015-5022.

Vilgelm, A. E., and Richmond, A. (2019). Chemokines Modulate Immune Surveillance in Tumorigenesis, Metastasis, and Response to Immunotherapy. *Frontiers in immunology* 10, 333.

Wu, V., Yeerna, H., Nohata, N., Chiou, J., Harismendy, O., Raimondi, F., Inoue, A., Russell, R. B., Tamayo, P., and Gutkind, J. S. (2019). Illuminating the Onco-GPCRome: Novel G protein-coupled receptor-driven oncocrine networks and targets for cancer immunotherapy. *J Biol Chem* 294, 11062-11086.

Yanagida, K., Kurikawa, Y., Shimizu, T., and Ishii, S. (2013). Current progress in non-Edg family LPA receptor research. *Biochim Biophys Acta* 1831, 33-41.

Yanagida, K., Masago, K., Nakanishi, H., Kihara, Y., Hamano, F., Tajima, Y., Taguchi, R., Shimizu, T., and Ishii, S. (2009). Identification and characterization of a novel lysophosphatidic acid receptor, p2y5/LPA6. *J Biol Chem* 284, 17731-17741.

Yasuda, D., Kobayashi, D., Akahoshi, N., Ohto-Nakanishi, T., Yoshioka, K., Takuwa, Y., Mizuno, S., Takahashi, S., and Ishii, S. (2019). Lysophosphatidic acid-induced YAP/TAZ activation promotes developmental angiogenesis by repressing Notch ligand Dll4. *The Journal of clinical investigation* 130, 4332-4349.

Yu, F. X., Zhao, B., Panupinthu, N., Jewell, J. L., Lian, I., Wang, L. H., Zhao, J., Yuan, H., Tumaneng, K., Li, H., *et al.* (2012). Regulation of the Hippo-YAP pathway by G-protein-coupled receptor signaling. *Cell* 150, 780-791.

Yung, Y. C., Stoddard, N. C., and Chun, J. (2014). LPA receptor signaling: pharmacology, physiology, and pathophysiology. *Journal of lipid research* 55, 1192-1214.

Figures

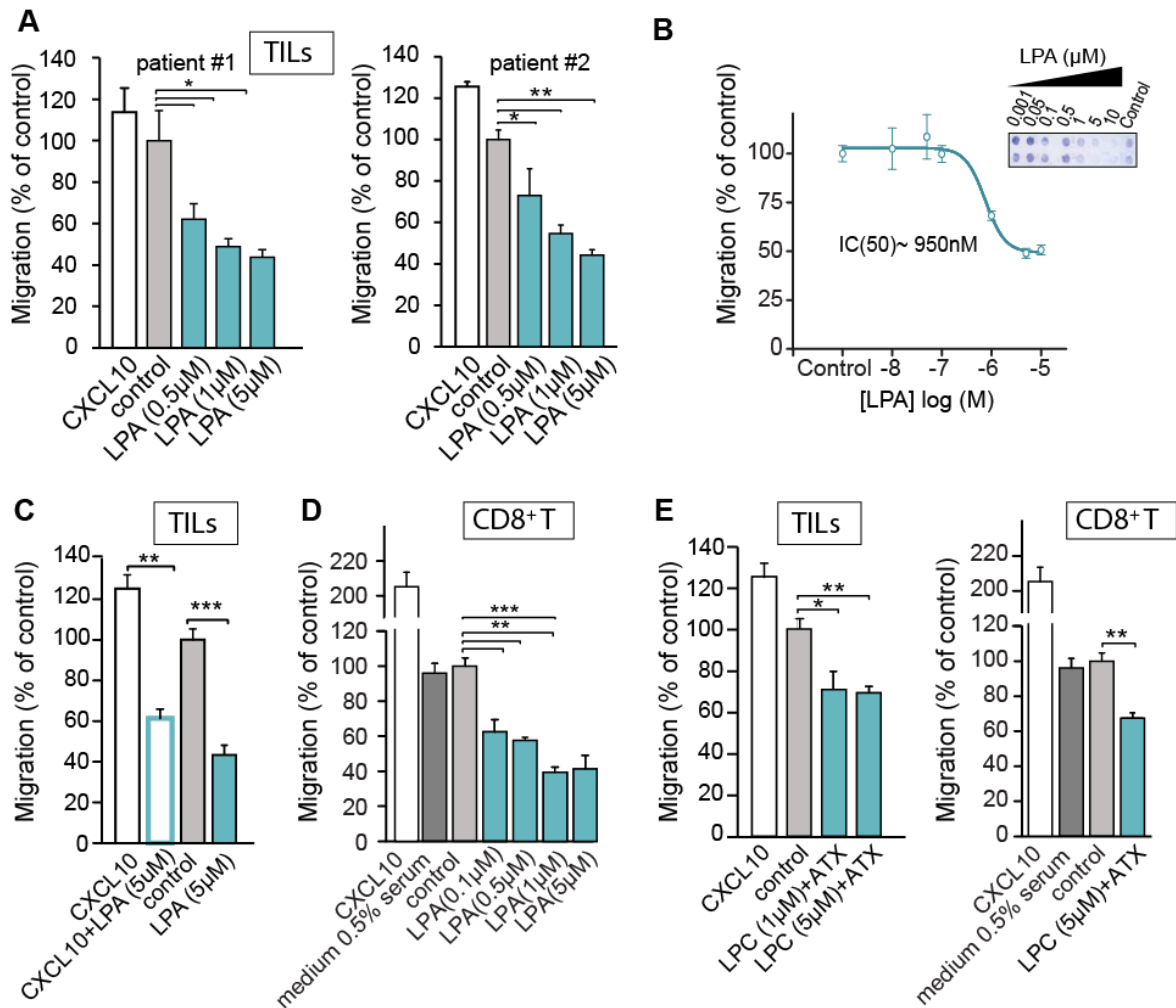


Fig. 1. LPA and ATX/LPC are chemorepulsive for TILs and CD8⁺ T cells

(A) Transwell migration of *ex vivo* expanded TILs from two melanoma patients stimulated with LPA(18:1) at the indicated concentrations. Chemokine CXCL10 (1 μM) was used as positive control. Agonists were added to the bottom wells and incubation was carried out for 2 hrs at 37°C.

(B) LPA dose-dependency. The inset shows a representative Transwell filter after staining. Migration was quantified by color intensity using Image J. Representative data of three independent experiments and values are expressed as mean ± SEM; *p<0.05 **p<0.01, unpaired t test.

(C) LPA overrules CXCL10-induced TILs chemotaxis. LPA(18:1) was added together with CXCL10 at the indicated concentrations. Data representative of two independent experiments, expressed as mean ± SEM; **p<0.01, ***p<0.001.

(D) Migration of CD8⁺ T cells isolated from peripheral blood, measured in the absence and presence of the indicated concentrations of LPA(18:1). Representative data from three independent experiments, expressed as mean ± SEM; **p<0.01, ***p<0.001 (t test, between the indicated groups). Note that the presence of 0.5% serum has no effect.

(E) Recombinant ATX (20 nM) added together with the indicated concentrations of LPC(18:1) recapitulates the inhibitory effects of LPA(18:1) on TILs and CD8⁺ T cells. Results are

representative of three independent experiments performed in triplicate, expressed as mean \pm SEM; * p <0.05 ** p <0.01 (unpaired t test).

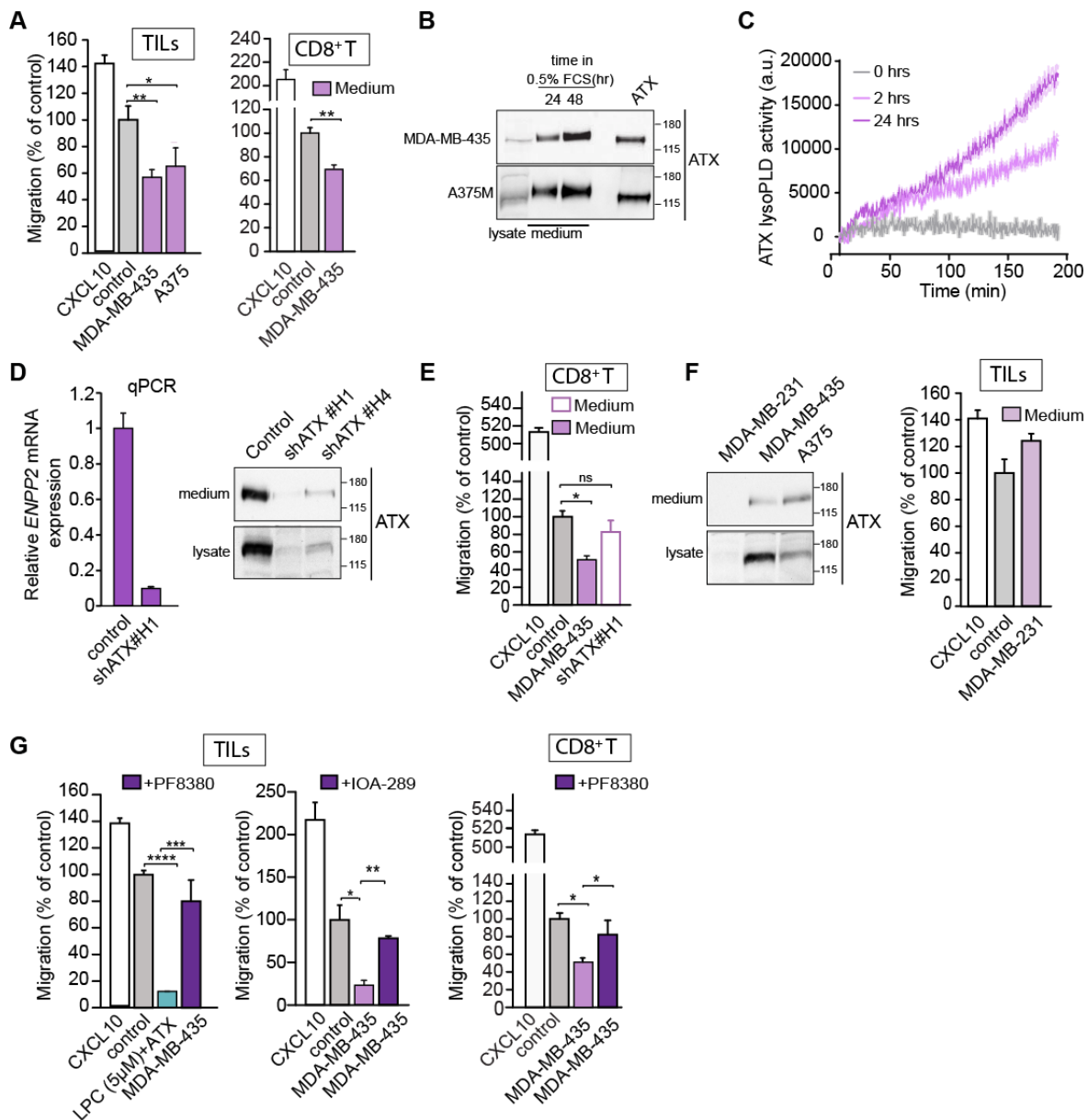


Fig. 2. ATX secreted by melanoma cells repels TILs and CD8+ T cells

(A) Melanoma-conditioned medium from MDA-MB-435 cells (collected after 24 hrs) is chemo-repulsive for TILs and CD8+ T cells. Experimental conditions as in **Figure 1**. Representative data of three independent experiments. Values are expressed as mean \pm SEM; * p <0.05 ** p <0.01 (unpaired t test).

(B) Immunoblot showing ATX expression in supernatants and cell lysates and from MDA-MB-435 and A375M melanoma cells. Cells were incubated in DMEM with 0.5% FCS for 24 or 48 hrs. Recombinant ATX (20 nM) was used as positive control (right lane).

(C) LysoPLD activity accumulating in melanoma-conditioned media over time. Medium from MDA-

MB-435 cells was collected after 2 and 24 hrs, and lysoPLD activity was measured as choline release from added LPC(18:1).

(D) Stable knockdown of ATX in MDA-MD-435 melanoma cells, as validated by qPCR and Western blot analysis.

(E) Medium from ATX knockdown MDA-MD-435 cells lacks chemorepulsive activity for CD8⁺ T cells. Data from a representative experiment. Values are expressed as mean \pm SEM; * $p < 0.05$ ** $p < 0.01$ (unpaired t test).

(F) Media from ATX-deficient MDA-MB-231 breast carcinoma cells lack chemorepulsive activity for TILs when compared to melanoma cell-conditioned media. *Left panel*, ATX immunoblots from the indicated media and cell lysates.

(G) Restoration of the migration of TILs and CD8⁺ T cells exposed to melanoma cell-conditioned media by ATX inhibitors, PF-8380 and IOA-289. Data represent a representative experiment (from three experiments using PF-8380 and two experiments using IOA-289). Values are expressed as mean \pm SEM; * $p < 0.05$ ** $p < 0.01$, *** $p < 0.001$, **** $p < 0.0001$ (unpaired t test).

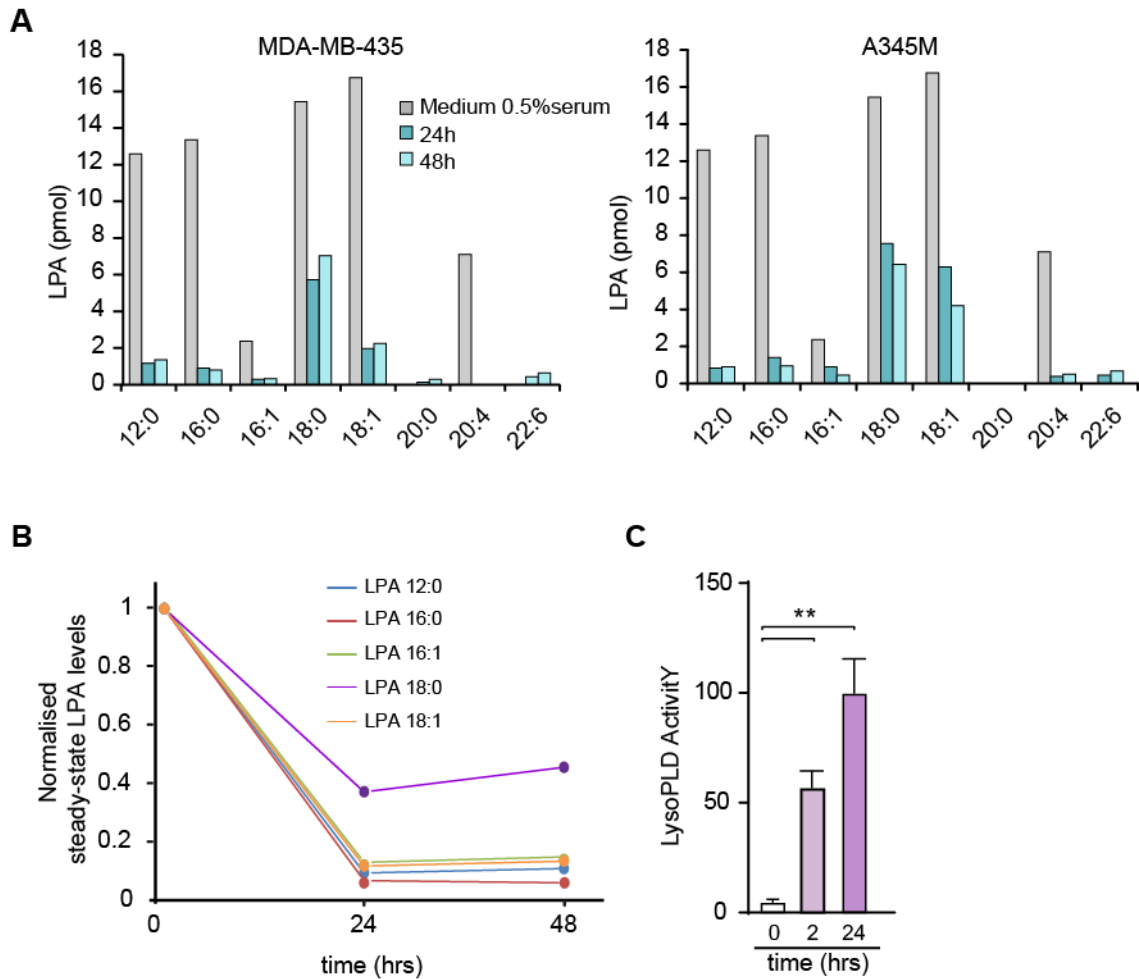


Fig. 3. Serum-borne LPA species and their rapid depletion by melanoma cells

(A) Determination of LPA species in conditioned medium from MDA-MB-245 and A375 cells, measured at T=0, 24 and 48 hrs, using LC/MS/MS. All media contained 0.5% FCS. Predominant serum-borne LPA species are (12:0), (16:0), (18:0), (18:1) and (20:4). Note LPA depletion from the medium within 24 hrs upon incubation with ATX-secreting melanoma cells.

(B) Time-dependent depletion of the indicated LPA species by melanoma cells.

(C) LysoPLD activity increases over time. Medium from MDA-MB-435 cells was collected after 2 and 24 hrs, and lysoPLD activity was measured as choline release from added LPC. Values are expressed as mean \pm SEM; ** p <0.01 (unpaired t test).

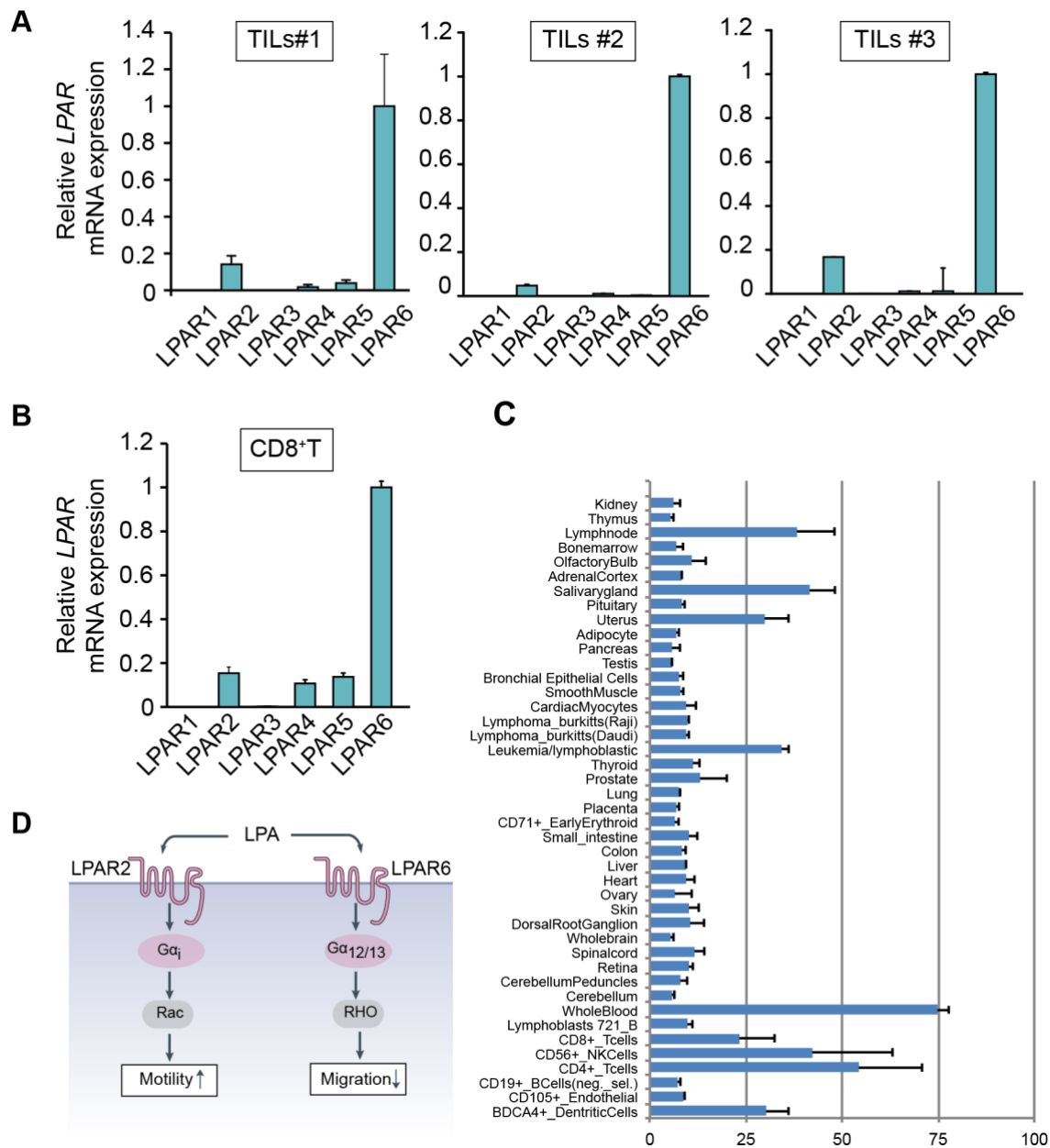


Fig. 4. LPAR expression levels in TILs and peripheral CD8⁺ T cells

(A) LPAR expression repertoire in *ex vivo* expanded TILs from three different patients (qPCR analysis relative to cyclophilin). Values are expressed as mean ± SD.

(B) LPAR expression in peripheral blood CD8⁺ T cells.

(C) LPAR6 expression in the indicated tissues and cell types. Note highest expression in lymphocytes. Data retrieved from <http://biogps.org>.

(D) Dominant G-protein signaling outcomes of LPAR2 versus LPAR6.

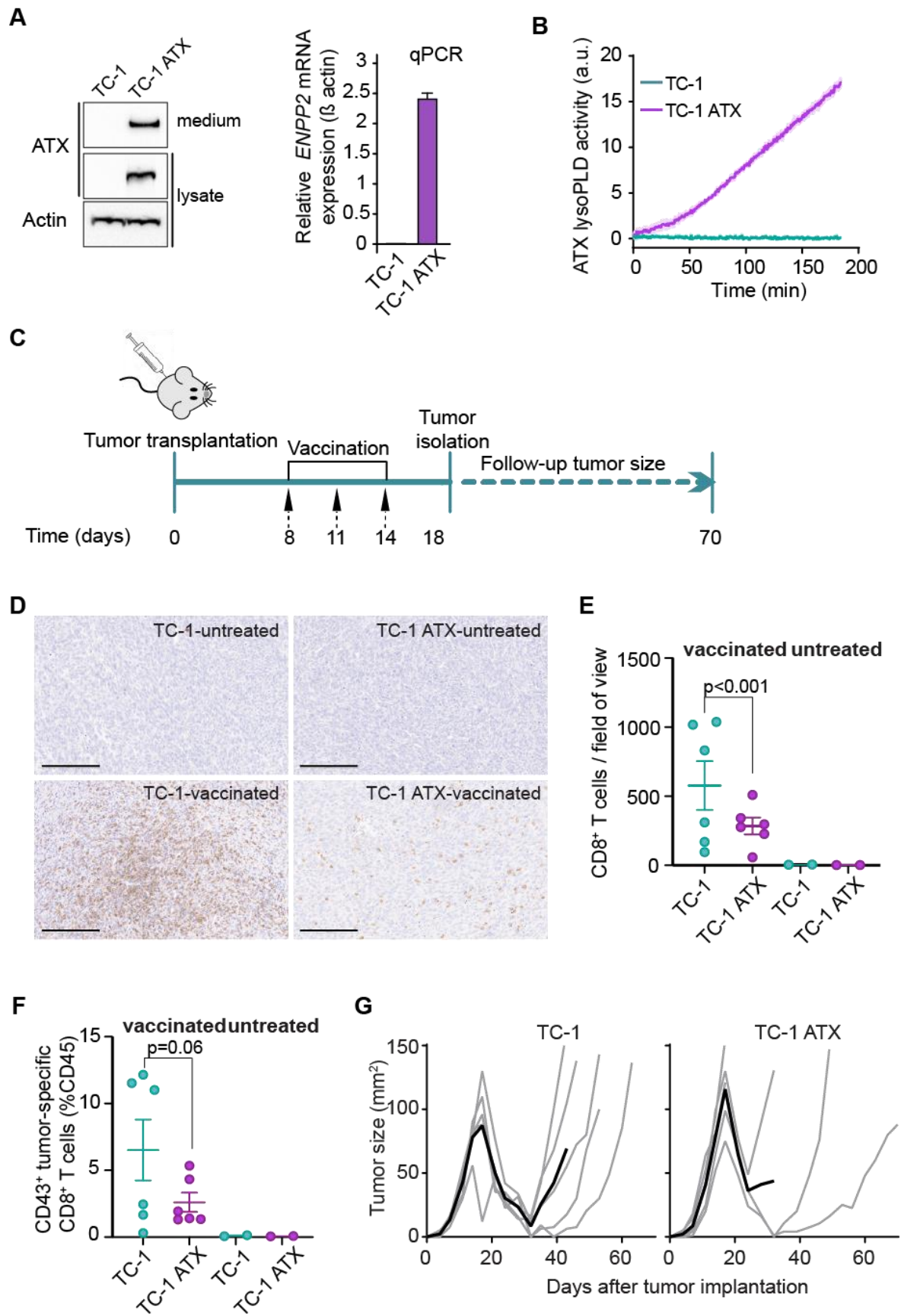


Fig. 5. ATX-secreting tumor cells suppress CD8+ T-cell infiltration in an anti-cancer vaccination model

(A) (Left) immunoblot analysis of ATX protein expression in TC-1 cells (TC-1) and TC-1 cells expressing ATX (TC-1 ATX). Actin was used as loading control. (Right) ATX expression (relative to Cyclophilin) in TC-1 and TC1-ATX cells analyzed by qPCR.

(B) ATX lysoPLD activity in supernatants from TC-1 and TC-1-ATX cells, as measured by choline release from added LPA(18:1) over time.

(C) Scheme of the experimental set-up in the anticancer vaccination model.

(D) CD8 immunostaining on tumor sections from untreated or vaccinated mice bearing wt- or ATX-expressing TC-1 tumors. Each image represents one representative field of view; scale bar, 200 μm .

(E) Quantification of CD8 immunostaining presented in **(D)**. Each data point represents the average of 4 (untreated mice) to 8 (vaccinated mice) fields of view of one mouse. Bar represents mean \pm SEM; *** $p < 0.001$.

(F) Flow cytometry quantification of the frequency of CD43+ (activated phenotype) E7₄₉₋₅₇ (RAHYNIVTF)-specific tetramer+ CD8+ cells present in the other half of the same tumors analyzed in **(D, E)**. Bar represents mean \pm SEM. $p = 0.06$ between vaccinated TC-1 and TC-1 ATX tumor-bearing mice. Means were compared using a Generalized Linear Model (see Methods).

(G) Tumor growth of mice bearing TC-1 and TC-1-ATX tumors, receiving the vaccination regimen presented in **(C)**. Grey lines represent individual mice; black lines represent the group average. Average tumor size was stopped when more than half the mice of each group had dropped out.

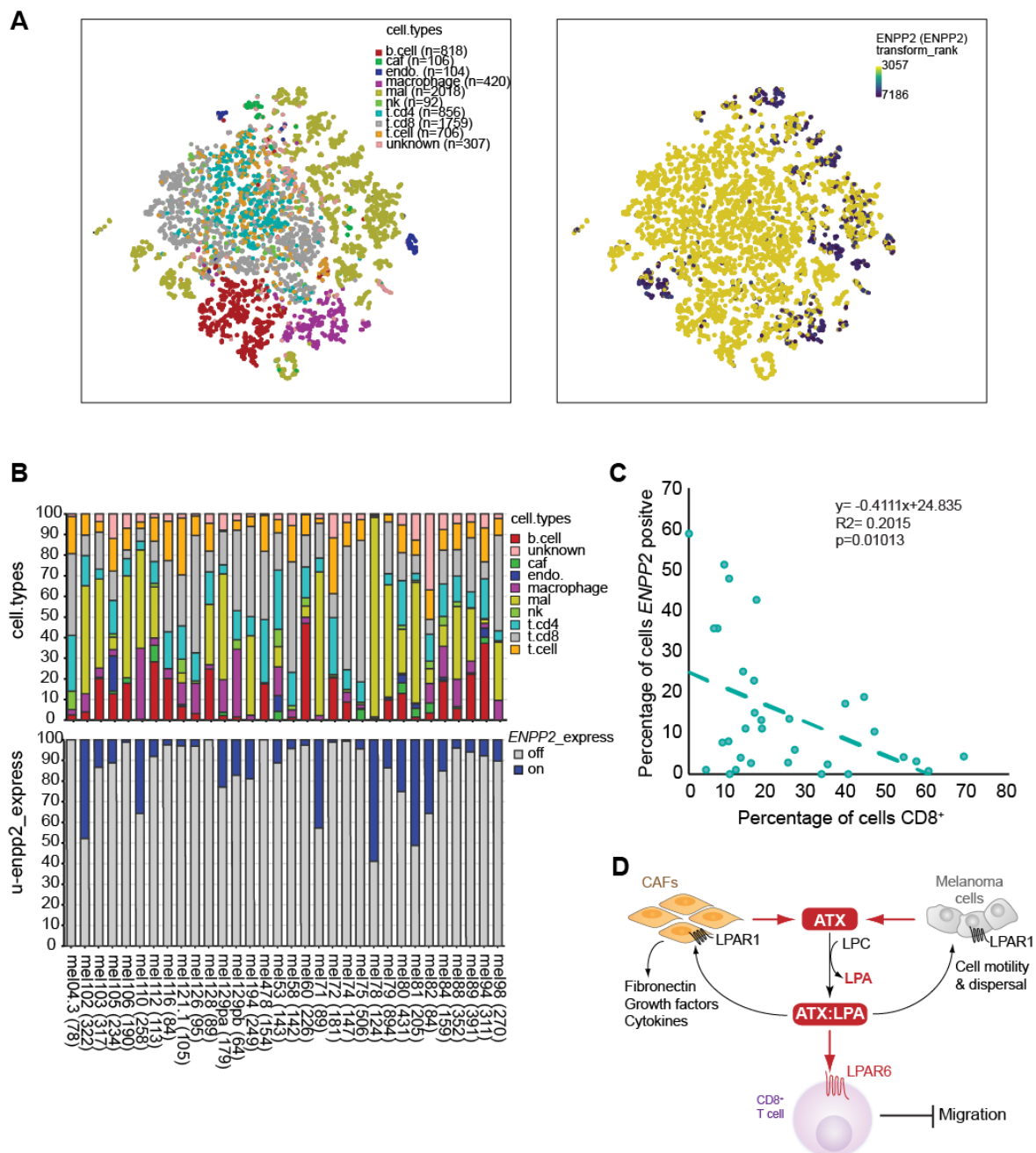


Fig. 6. Single-cell analysis of *ENPP2* expression in melanoma tumors and its negative correlation with $CD8^+$ T-cell accumulation

(A) tSNE embedding of 7186 single cells (perplexity = 5) from 32 melanoma patients (prior to immunotherapy) as described (Jerby-Arnon et al., 2018). Data were used to project patients, inferred cell types and \log_2 *ENPP2* expression values, respectively, as described in Methods. **Right panel** shows *ENPP2* expression (blue/purple dots high expression) as overlay on single cells presented in the **left panel**. Intratumoral *ENPP2* expression is detected in malignant cells (mal), cancer-associated fibroblasts (caf), macrophages and endothelial cells (endo), but not in lymphocytes (T, B and NK cells).

(B) Stacked bar graph showing the percentages of inferred cell type per individual patient sample (top), and the percentage of *ENPP2*-expressing cell types (bottom).

(C) Negative correlation of intratumoral *ENPP2* expression and CD8⁺ T-cell accumulation. Pearson correlation between the percentage of inferred *ENPP2*-expressing cells and CD8⁺-positive cells ($r=0.4$; $p=0.01$).

(D) In the melanoma microenvironment, ATX is secreted by melanoma cells and diverse stromal cells, particularly fibroblasts (CAFs), to convert LPC into LPA. ATX functions as a chaperone (ATX:LPA) that carries LPA to its GPCRs and exerts dual actions: it suppresses T-cell infiltration through LPAR6, while it promotes melanoma cell dispersal and activates CAFs via LPAR1, as schematically highlighted. Besides antagonizing T-cell infiltration, LPAR stimulation evokes an early gene expression signature in TILs, the functional consequences of which are currently unknown (**Fig. S2A,B**). See text for further details.

Supplemental Information

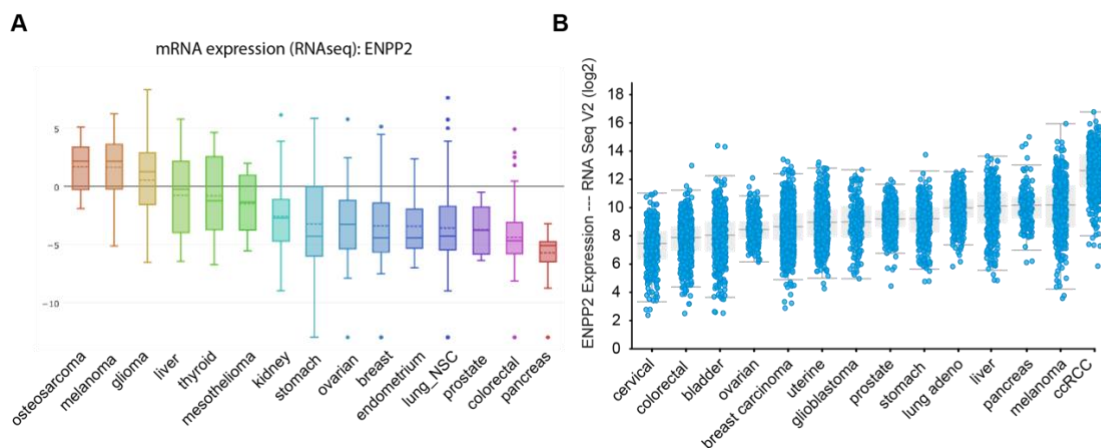


Fig. S1. *ENPP2* expression analysis

(A) *ENPP2* expression in the indicated cancer cell lines ranked according to median values. Note high *ENPP2* expression in melanoma cell lines ($n=61$). RNAseq expression data were retrieved from the Cancer Cell Line Encyclopedia (CCLE)(Ghandi et al., 2019).

(B) Pan-cancer analysis of *ENPP2* expression in the indicated solid tumors ranked according to median values. RNAseq v2 mRNA expression data were retrieved from the TCGA database (<https://www.cbiportal.org>).

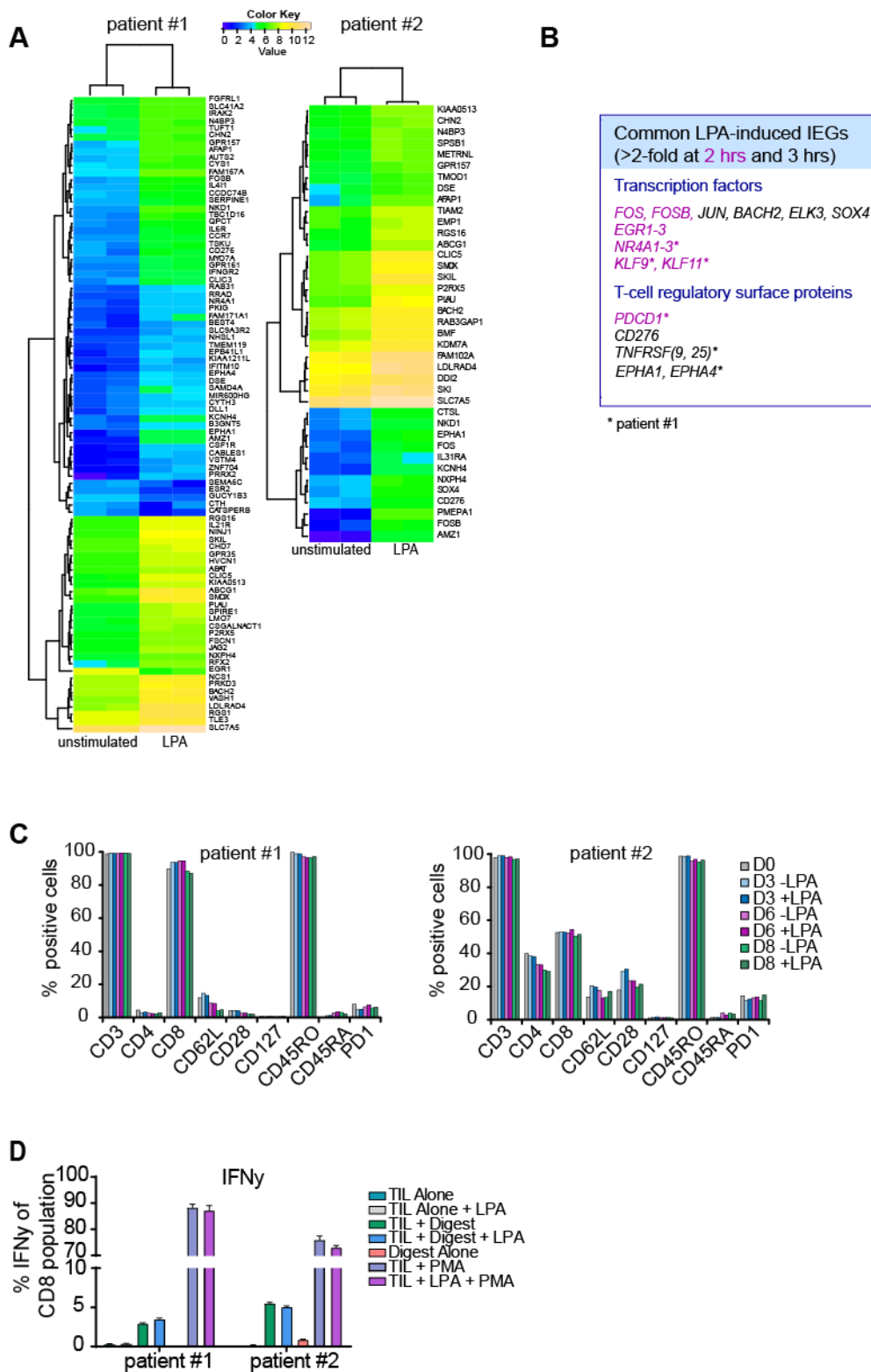


Fig. S2. LPA-regulated early genes and phenotypes in melanoma TILs

(A) Heat maps of differentially expressed genes in LPA-treated TILs from two melanoma patients as determined by RNA-seq (cutoff $\log_2FC=1.5$; $p<0.001$). TILs maintained on low serum were

treated with LPA (5 μ M) for 3 hrs. Note marked differences between both patients. Experiments were performed in duplicate, as indicated.

(B) Selected common LPA-induced immediate early genes (IEGs) after 2 hrs and 3 hrs, indicated in red and black respectively (cutoff $\log_2FC=1.0$). Corresponding heat maps not shown for convenience. Primary RNA-seq data are deposited at GEO, accession number GSE143697.

(C) Expression of the indicated T-cell phenotypic markers was analyzed by flow cytometry in TILs before and after treatment with LPA (5 μ M) up to 8 days.

(D) Intracellular production of IFN- γ upon co-incubating TILs with matching autologous melanoma cells under the indicated conditions. Phorbol ester, PMA (1 μ M), was used as a positive control. See Methods for details.

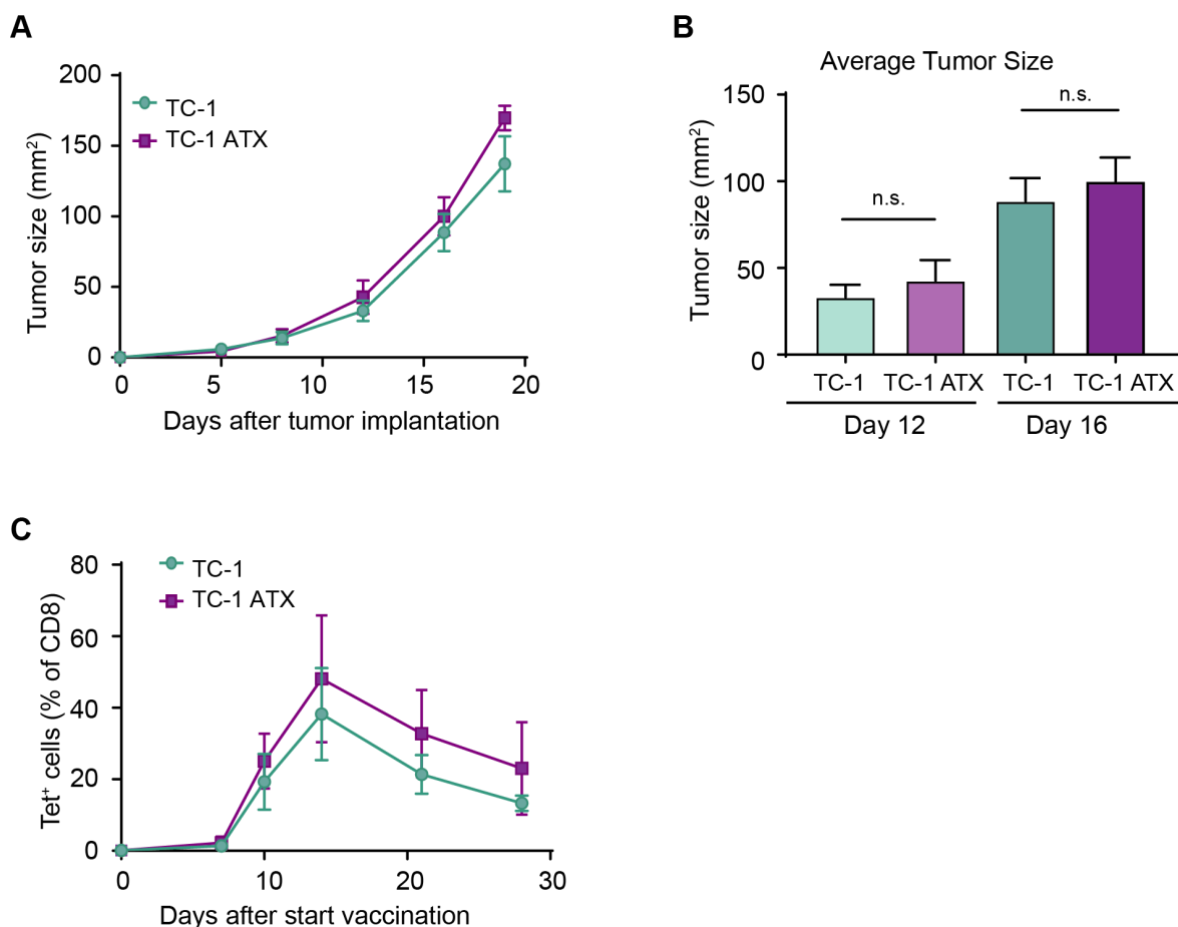


Fig. S3. Tumor growth and CD8⁺ T cell response in the TC-1 model

(A) Tumor growth in mice bearing ATX-deficient versus ATX-expressing TC-1 tumors.

(B) Average tumor size of mice from **(A)** on days 12 and 16 after tumor implantation.

(C) Tetramer-positive cells in blood of TC-1 and TC-1-ATX tumor-bearing mice, vaccinated with DNA encoding E7 tumor antigen and helper epitopes on day 0, 3 and 6 (Day 0 of vaccination corresponds to Day 9 after tumor implantation).